Article

Bias Correction of Chinese Fengyun-3C Microwave Humidity and Temperature Sounder Measurements in Retrieval of Atmospheric Parameters

Qiurui He [1,2], Zhenzhan Wang [1,*] and Jieying He [1]

[1] Key Laboratory of Microwave Remote Sensing, National Space Science Center, Chinese Academy of Sciences, Beijing 100190, China; heqiurui@126.com (H.Q.); hejieying@mirslab.cn (H.J.)

[2] University of Chinese Academy of Sciences, Beijing 100049, China

* Correspondence: wangzhenzhan@mirslab.cn; Tel.: +86-10-6258-6454

Abstract: The Microwave Humidity and Temperature sounder (MWHTS) on board the Fengyun (FY)-3C satellite measure the outgoing radiance form the Earth surface and atmospheric constituents. MWHTS makes measurements in the isolated oxygen absorption line near 118 GHz and the vicinity of strong water vapor line around 183 GHz, can provide fine vertical distribution structure of both atmospheric humidity and temperature. However, in order to obtain the accurate soundings of humidity and temperature by the physical retrieval method, bias between the observed radiance and those simulated by radiative transfer model from the background or first guess profiles must be correct. In this study, two bias correction methods are developed through the correlation analysis between MWHTS measurements and air mass identified by the first guess profiles of the physical inversion, one is the linear regression correction (LRC) and the other is neural networks correction (NNC), representing the linear and nonlinear nature between MWHTS measurements and air mass, respectively. Both correction methods have been applied to MWHTS observed brightness temperatures over the geographic area (180° W-180° E, 60° S-60° N). The corrected results are evaluated by the probability density function of the difference between corrected observations and simulated values and the root mean square error (RMSE) with respect to simulated observations. The numerical results show that the NNC method perform better, especially in MWHTS channels 1 and 7-9 whose peak weight function heights are close to the surface. In order to assess the effects of bias correction methods proposed in this study on the retrieval accuracy, a one-dimensional variational system was built and applied to the MWHTS uncorrected and corrected brightness temperatures to estimated atmospheric temperature and humidity profiles, The retrieval results show that the NNC has better performance which is to be expected. An indication of the stability and robustness of NNC method is given which suggests that the NNC method has promising application perspectives in the physical retrieval.

Keywords: FY-3C/MWHTS; linear regression correction; neural networks correction; one-dimensional variational algorithm; atmospheric temperature and humidity profiles

1. Introduction

Atmospheric temperature and humidity profiles play important roles in wide range of atmospheric applications, such as climate monitoring, weather forecasting, initialization and evaluation of numerical weather prediction (NWP) models, assessing the atmospheric stability and nowcasting the intense convective weather to name a few [1,2]. Such profiles can be retrieved from observations taken by satellite-borne sounders. Microwave measurements are advantageous over visible or infrared because clouds do not absorb and scatter microwave radiation to the same degree [3]. This allows for microwave measurements of atmospheric parameters in most weather conditions, and provide a substantial data set [4]. FY-3C, launched in September 2013, is the

second-generation polar-orbiting meteorological satellite. The MWHTS on board FY-3C has 15 channels at frequency ranging from 89 to 191 GHz which allows for simultaneously retrieving the atmospheric temperature and humidity profiles with good temporal and spatial sampling under clear and cloudy conditions [5]. MWHTS inherited most of the channels from its predecessors: microwave humidity sounder onboard FY-3A and FY-3B satellites. However, MWHTS includes eight new temperature sounding channels centered at 118.75 GHz oxygen absorption line which are used in operation for the first time internationally, and two new water vapor sounding channels, provides more details of vertical distribution structure of atmospheric temperature and humidity.

Although the development of atmospheric temperature and humidity profiles measured by satellite-borne sounders has a history of over 50 years and improvement of this important inversion approach is actively continuing [6], the retrieval strategies can be put into two categories which term statistical methods and physical methods. Statistical approaches essentially use a statistical relationship between the actual observations and the atmospheric state variables which do not take into account any physical models [7,8,9,10]. However, in essence, physical methods propagate a first guess of the atmospheric parameters through a radiative transfer model and an iterative scheme, numerical procedures to fit the simulated measurements to the satellite observations by updating the first guess at each iteration [11,12,13,14]. Physical methods are the basic way to improve the retrieval accuracy, and have been widely adopted, since they have clear physical meanings. All of the physical methods employ either a minimum variance estimate or maximum likelihood estimate under the assumption that observations are unbiased and have Gaussian errors [15]. Any bias related to the instrument and the radiative transfer model should be taken into account when determining the appropriate weight to give to the radiance data in the physical retrieval process, therefore it must be quantified and removed. The term bias in our study refers to error that is systematic rather than random. In statistics, bias is a nature of an estimator which, on average, over- or underestimates the true value. For instance, a radiative transfer model which is always cold under certain circumstances is biased [16]. Biases in the observations and the radiative transfer model arise duo to systematic errors in any one (but generally a combination) of the following sources: the satellite sounder itself (e.g. poor calibration, or adverse environmental effects); the radiative transfer model linking the atmospheric parameters to the radiation measured by the satellite (e.g. errors in the physics or spectroscopy, or from non-modeled atmospheric process); and errors in the background atmospheric parameters from some data sources (e.g. radiosonde observations, Numerical Weather Prediction (NWP) analyses, climate re-analyses, etc) [17]. Since the causes of bias are complicated and manifold, it is very hard to remove bias in purely physical term. Many efforts based on statistical methods have been made to develop bias correction scheme for the NWP radiances assimilation system and the physical retrieval system based on the variational approach. This two systems sharing the same basis which is the minimization of a similar cost function to find the optimal solution can share the same radiometric bias removal. Many previous studies have developed empirical correction methods which remove the systemic biases by an empirical corrected varying with instrument itself, radiative transfer model, observation conditions, etc [18-20]. Li et al. adjust the observations or forward model calculations by statistical relationships between the radiances of corresponding channels irrespective of atmosphere state [21]. However, Kelly and Flobert, McMillin et al. and Uddstrom demonstrated that a successful bias correction scheme must taken into amount the spatially varying and air mass dependent nature of the radiance biases, and proposed the scan correction which make a correction for the relative mean bias between measurements at different scan angles, and air-mass correction taking into account the air-mass dependent nature of the radiance biases [22-25]. Based on air-mass correction, in satellite radiances assimilation system, adaptive bias correction scheme has been proposed which can distinguish the observation biases from the biases in the background in order to prevent the analysis from drifting towards its own climate [26-29]. However, all these air mass correction schemes belong to the linear regression approach assuming that the relationship between the atmospheric state and radiance bias is linear which may not represents the intrinsic features between them very well.

To correct the biases between observations and those simulated by radiative transfer model in physical retrieval procedure, for air-mass correction, the linear regression correction (LRC) and neural networks correction (NNC), representing the linear and nonlinear relationships between the biases in MWHTS measurements and air mass respectively, were proposed. In order to evaluate the performances of this two bias correction methods, a one-dimensional variational retrieval system was built to retrieve atmospheric temperature and humidity profiles using MWHTS brightness temperatures to investigate the effect of this two different correction approaches on retrieval accuracy. In addition, the tests of the stability and robustness of correction method proposed in this study were carried out by comparing to different atmospheric conditions and over different algorithm initialization conditions. This paper is organized as follows: Section 2 will present the major instrument characteristics of FY-3C/MWHTS. Radiative transfer model simulations of brightness temperatures are describe and LRC and NNC approaches for the air mass correction and scan correction are proposed in Section 3. The retrieval system for MWHTS data is built and its implementation in Section 4. The proposed bias correction approaches are evaluated in Section 5. Finally, conclusions are summarized in Section 6.

2. Description of MWHTS instruments characteristics

On 23 September 2013, the FY-3C satellite was successfully launched into a circular, near-polar, morning-configured (1005 LT) orbit with an altitude of 836 km above the earth and an inclination angle of 98.75° to the equator. MWHTS on board FY-3C is a total power radiometer, has a cross-track scanning geometry within ±53.35° with respect to the nadir direction. MWHTS completes one scan every 2.66 s and its swath is 2645 km, giving a nominal field of view (FOV) of 16 km at nadir. Each scan line has 98 FOVs together with a view of cold space and the onboard warm calibration target, used to perform a two-point radiometric calibration [30]. MWHTS has 15 channels with 8 temperature sounding channels for measuring temperature from surface to the upper atmosphere, 5 humidity sounding channels for measuring water vapor and liquid precipitation in the troposphere from surface to about 300 hPa, two window channels for providing information on the surface characteristics. Table 1 lists some of the channel characteristics of the FY-3C/MWHTS, including channel frequency, polarization, bandwidth, sensitivity of channel as measured in flight, peak weighting function (WF) height.

Figure 1 displays the WF distributions for 15 channels of MWHTS calculated from a standard U.S. atmospheric profile at nadir by Millimeter-wave Propagation Model (MPM)-93 [31]. The WFs indicate the relative contribution of each atmospheric layer to the observations. For a given instrument channel and atmosphere state, the peak WF height increases with increasing zenith angle, since the optical path length sounded by the satellite increased with the instrument scan angles [32]. It is seen that MWHTS channels 1-9 measure the atmospheric temperature form the surface to 30 hPa, mainly in the stratosphere. MWHTS channels 10-15 measure the humidity in the troposphere. The WFs for MWHTS channels 7-9 in the far wing region of 118.75 GHz oxygen absorption line and MWHTS channels 1, 10 near the atmospheric absorption window have their maximum closer to the surface, these channels are affected by the radiation from both the surface and the boundary layer and can be used to obtain Earth's surface information.

In our study, level 1b MWHTS brightness temperatures are used have been obtain from National Satellite Meteorological Center (http://www.nsmc.cma.gov.cn/NSMC/HOME/Index.html). The MWHTS brightness temperatures converted from calibration data using non-linear correction and correction of antenna spill-over effects have been validated by Guo [5].

Preprints (www.preprints.org) | NOT PEER-REVIEWED | Posted: 19 August 2016 doi:10.20944/preprints201608.0178.v1

Peer-reviewed version available at Atmosphere 2016, 7, 156; doi:10.3390/atmos7120156

Table 1. MWHTS channel characteristics

Channel	Frequency (GHz)	Polarization	Bandwidth (MHz)	Peak WF (hPa)	Sensitivity of MWHTS as measured in flight (K)
1	89.0	V	1500	Window	0.23
2	118.75±0.08	H	20	30	1.62
3	118.75±0.2	H	100	50	0.75
4	118.75±0.3	H	165	100	0.59
5	118.75±0.8	H	200	250	0.65
6	118.75±1.1	H	200	350	0.52
7	118.75±2.5	H	200	Surface	0.49
8	118.75±3.0	H	1000	Surface	0.27
9	118.75±5.0	H	2000	Surface	0.27
10	150.0	V	1500	Window	0.34
11	183.31±1	H	500	300	0.47
12	183.31±1.8	H	700	400	0.34
13	183.31±3	H	1000	500	0.3
14	183.31±4.5	H	2000	700	0.22
15	183.31±7	H	2000	800	0.27

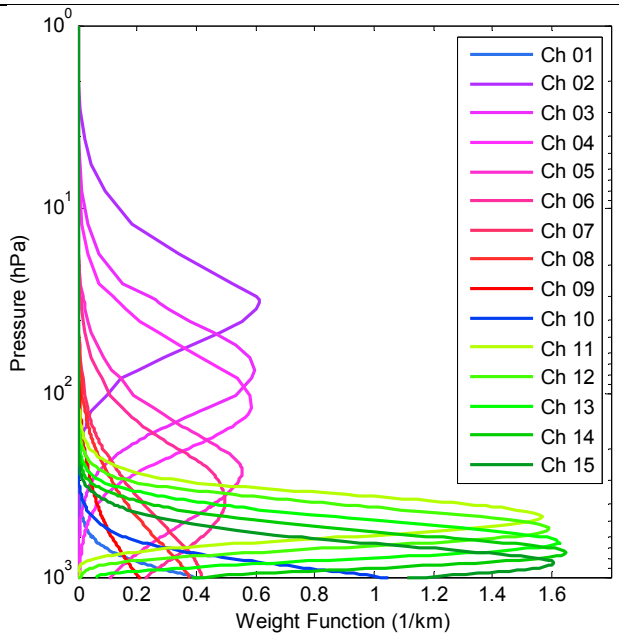

Figure 1. Weight functions for the 15 channels of FY-3C/MWHTS calculated from the U.S. standard atmospheric profile at nadir, assuming a surface emissivity of 0.6.

3. Forward model and bias correction

3.1. Forward model simulations

Emission, absorption and scattering of radiation at microwave frequencies by the atmospheric constituents are the physical basis for measuring the atmospheric parameters, such as temperature or humidity. The radiation at the top of the atmosphere measured by a radiometer on board satellite can be simulated by a radiative transfer model [33]. In the process of physical retrieval, it is necessary to compare observed and simulated measurements, and the radiative transfer model is an essential part of the physical retrieval algorithm. In this study, The fast radiative transfer model RTTOV (Radiative Transfer for Television and Infrared Observation Satellite Operational Vertical Sounder), version 11.2 developed by the European Center for Medium-Range Weather Forecast (ECMWF) is used to simulate MWHTS brightness temperatures. Because the surface emissivity has a serious impact on the microwave upwelling radiation, it must be taken into account in radiative

transfer simulations [34]. For MWHTS, the surface emissivity affects the measurements of the two window channels 1,10 ,temperature sounding channels 7-9 and water vapor sounding channel 15 whose peak WF heights are closer to the surface. In RTTOV v11.2 [35], over ocean, the surface emissivities are computed by the FASTEM-5 model [36], over land, A Tool to Estimate Land-Surface Emissivities at Microwave frequencies (TELSEM) emissivity atlas is used [37].

ERA-Interim produced by a data assimilation system including a 4-dimensional variational analysis with a 12-hour analysis window, which assimilate many sounding measurements including radiosondes and in situ sounders, is a reanalysis of the global atmosphere at ECMWF, will be used as inputs to RTTOV to simulate MWHTS observations in our study. For a detailed documentation of the ERA-Interim Archive see Berrisford et al. [38]. This data set with horizontal resolution of 1°×1° and temporal resolution of 6 h (i.e., with data available at 0000 UTC, 0600 UTC, 1200 UTC and 1800 UTC) is selected in this work, the profile parameters of which has a total of 37 pressure levels unevenly spaced from 1000 hPa to 1 hPa. The profiles of temperature, humidity and cloud liquid water and the surface parameters including surface pressure, 10 m wind speed, 2 m dewpoint temperature, 2 m temperature and skin temperature are used as inputs to RTTOV. Due to lack of accurate information about cloud ice and rain parameters from the ERA-Interim, simulations are carried out by the emission-based model neglecting scattering from clouds and precipitation in RTTOV. Since ice and snow emissivity is not well characterized in the RTTOV [33], which can strongly contribute to the uncertainty in the simulations, only ERA-Interim data covering geographic area (180° W-180° E, 60° S-60° N), where is ice-free surface, were utilized.

In order to remove the systematic biases in MWHTS observations, it must be construct a matchup file, which contains the time and space collocated MWHTS observations, simulations from RTTOV and ERA-Interim reanalysis data set, to compare simulated and observed measurements. The criteria for collocating MWHTS observations with ERA-Interim data are that the time difference between ERA-Interim reanalysis data and MWHTS observations is less than 0.5 h, and the absolute distance between the position (latitude and longitude) of ERA-Interim reanalysis data and MWHTS observations is less the 0.5°. It is worth noting that simulations from RTTOV does not taken into account scattering from clouds and precipitation, thus it is necessary to filter out the cloudy MWHTS observations which are affected by a cloud with a high ice content, precipitating cloud and precipitation. In our study, we use the cloud filtering method developed by Buehler [39], which using measurements at 183.31±1.00 GHz and the difference of measurements at 183.31±1.00 GHz and 183.31±3.00 GHz to create a threshold to filter out the cloudy observations. For a detailed description of the cloud filtering methodology see Buehler et al. and Burns et al. [39-42]. For MWHTS, the criteria of filtering out cloudy observations are that the brightness temperature difference between channels 11 and channel 13 is greater than zero and the brightness temperature of channel 11 is greater than 240.6 K. Based on the collected criteria and the cloudy observations filtering criteria, two collocated datasets have been generated, one is the statistical analysis dataset with 254612 collocated samples over land and 1393744 collocated samples over ocean from 1 February to 31 May 2014, is used to analyze the bias characterization of MWHTS and train the statistical algorithms. The other is the testing dataset with 67652 collocated samples over land and 345039 collocated samples over ocean from 1 to 30 June 2014, is used to evaluate the algorithm performance.

3.2. Bias correction

For FY-3C/MWHTS measurements, the bias can be put into two categories, scan bias which changes with scan angle of instruments, and air-mass bias which tends to vary with the air mass and surface characteristics of the earth. In our study, the bias correction scheme is a two-step process, scan correction and air-mass correction. The bias correction can be carried out by either adjusting the satellite measurements or the simulated calculation [21]. In general, the satellite measurements are adjusted for use to avoid bias correction at each iteration in the physical retrieval procedure.

Preprints (www.preprints.org) | NOT PEER-REVIEWED | Posted: 19 August 2016 doi:10.20944/preprints201608.0178.v1

Peer-reviewed version available at Atmosphere 2016, 7, 156; doi:10.3390/atmos7120156

3.2.1. Scan correction

Though the simulated calculations from RTTOV have been take into account the scan angle of instrument, which scans in a cross-track manner, residual biases vary with scan positions obviously in the MWHTS measurements, and the biases display noticeable variations in space. Dividing statistical analysis dataset according to latitude band, in this case every 10°, to calculate the mean bias between the observed and simulated values:

$$d_j(\phi,\theta) = \bar{O}_j(\phi,\theta) - \bar{S}_j(\phi,\theta), \quad (1)$$

where d is the mean bias, $\bar{O}$ is the averaged observed brightness temperatures, $\bar{S}$ is the simulated brightness temperatures, θ is the scan angle, ϕ is the latitude band and j is the channel. Taking MWHTS channel 4 for example, Figure 2 shows the distribution of the mean bias by latitude band at 98 scan positions. It can be seen that the biases varies significantly with scan positions, particularly at the first 10 scan angles. In addition, the biases at different latitude band are more or less different, the maximum and minimum of which differ by about 2 K.

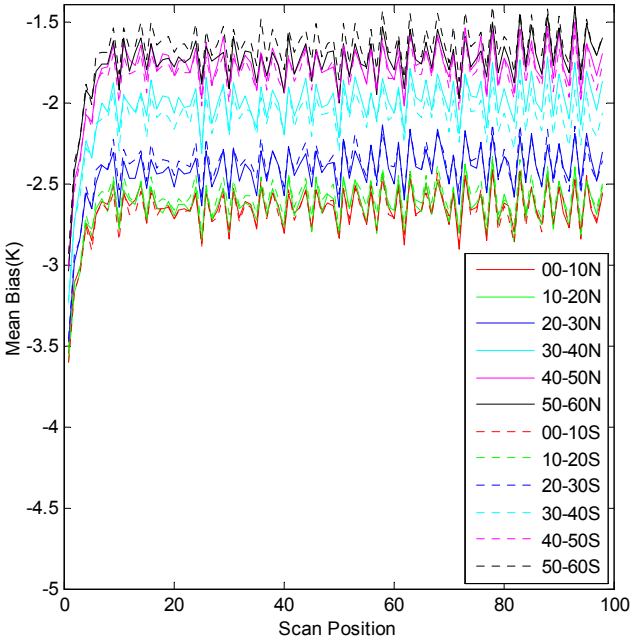

Figure 2. Scan bias by latitude band, FY-3C/MWHTS channel 4.

On the basis of these studies, the scan correction can be divided into 12 latitude bands of 10° of longitude. However, correction coefficients across latitude bands may be not continuous, thus some smoothing is required. In our study, a simple smoothing approach is carried out to generate a smooth transition between latitude bands as described by Harris et al. [25]. The smoothing is given by

$$d'_j(\phi,\theta) = \frac{1}{4}d_j(\phi-1,\theta) + \frac{1}{2}d_j(\phi,\theta) + \frac{1}{4}d_j(\phi+1,\theta), \quad (2)$$

$d_j(\phi,\theta)$ are averaged by the sampling method.

3.2.2. Air-mass correction

Bias in the radiative transfer model, because of errors in the physics or spectroscopy, or from imprecise modeling of the atmospheric process, is relate to the atmospheric state sounding by the satellite. Removing this bias in physical terms is difficult, in generally, predicting it using statistic method with bias predictors is preferred. In order to identify the air mass which can provided a

Preprints (www.preprints.org) | NOT PEER-REVIEWED | Posted: 19 August 2016 doi:10.20944/preprints201608.0178.v1

Peer-reviewed version available at Atmosphere 2016, 7, 156; doi:10.3390/atmos7120156

good representation of the atmospheric state, MWHTS observation bias/temperature and bias/humidity correlations which can be used to study which combinations of atmospheric variables could be taken as bias predictors are calculated at each pressure level using the statistical analysis dataset complied in section 3.1. These correlations show in Figure 3. For temperature, it can be seen that there is a correlation between MWHTS brightness temperature bias and the layer 1000-200 hPa, 200-50 hPa and 20-1 hPa for channels 2-5 and channels 11-14, but the correlation is very weak for channels 6-10. The humidity correlations are displayed for most of channels in the layers 1000-100 hPa as shown in Figure 3(b). In addition, there is a high correlation between the surface temperature and channels 4. However, it is surprising that the temperature sounding channel 6-9 show little correlation for brightness temperature bias/temperature correlations, the humidity sounding channels show weaker correlation than most of temperature sounding channels for brightness temperature bias/humidity correlations, and window channels 1 and 10 which sense the surface do not shows high correlation at surface. It is important to realize that we are talking about the bias, not the brightness temperature themselves. It does not necessarily follow weight functions as Figure 2 shows that if a channel senses a given atmosphere layer, that the bias will depend on this layer, the bias may be caused by another layer, because of correlations present in different layers of the atmospheric temperature and humidity [25].

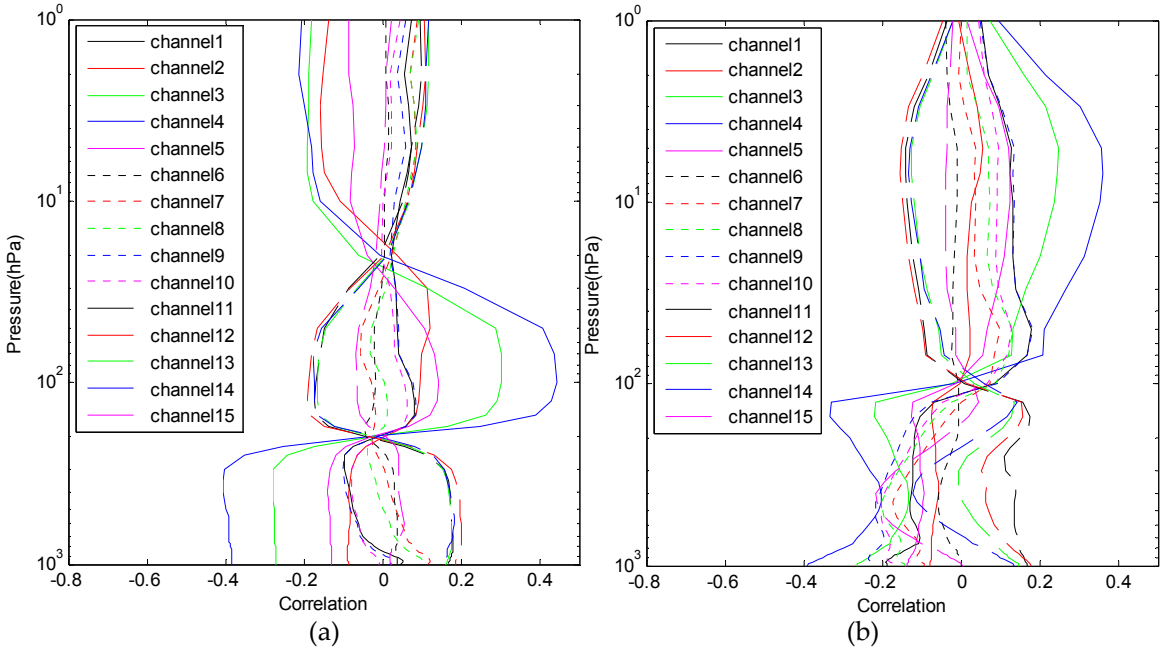

Figure 3. Atmospheric parameters-bias correlations, MWHTS channels 1-15: (a) temperature-bias, (b) humidity-bias.

As a result of this correlation analysis, we can find that a certain correlation is exist between the bias and air mass, but is not significant, especially for channels 6-9 for temperature. In our study, we proposed two correction methods, air-mass LRC and NNC, representing the linear and nonlinear relationship between MWHTS observation bias and air mass, respectively.

1. LRC method

The air-mass regression correction assuming a linear relationship between the brightness temperature bias and the air mass uses a set of bias predictors to predict the bias through the following equation [25]:

$$Z_j = \sum_{i=1}^{n} A_{ji} X_i + C_j, \quad (3)$$

where j is the channel, $X_i (i = 1,...,n)$ is the bias predictors, A_{ji} and C_j are the coefficients which are computed by carrying out a least-squares fit on data samples containing the brightness temperature bias and its corresponding air mass representing the atmospheric state. The coefficients A_{ji} are given by

$$A_{ji} = \sum_{k=1}^{n} \langle D_j, X_k \rangle \bullet \left[\langle \boldsymbol{X}, \boldsymbol{X} \rangle \right]_{ki}^{-1}, \tag{4}$$

where the< > denote covariances, $\boldsymbol{X}$ is the vector X_i, D_j is the same as $d_j'(\phi,\theta)$ in formula (2). The coefficients C_j are given by

$$C_j = -\bar{d}_j' - A_{ji}^{\,T} \bullet \bar{\boldsymbol{X}}. \tag{5}$$

where T represents matrix transpose, the over bar represents the mean.

For the bias predictors X_i, after some testing, the best combination of predictors would be：1000-200 hPa thickness, 200-50 hPa thickness, 20-1 hPa thickness, surface skin temperature and column water vapor. In our study, X_i is construct using the atmospheric temperature and humidity profiles and surface skin temperature in the statistical analysis dataset complied in section 3.1, along with the corresponding differences of observations and simulations to calculate the coefficients in this linear regression algorithm.

2. NNC method

neural networks (NNs) are massively parallel and distributed structures inspired by biological networks of densely connected neurons, each of which can do computations. Just as biological NNs can learn from their environment, NNs have the ability to learn from the presentation of training data, as weights and biases of which can be tuned to fit the training data adaptively. In recent years, NNs are widely used in the retrieval of atmospheric geophysical parameters using remote sensing data, as NNs can be used to learn and compute function for which the analytical relationships between inputs and outputs are complex, especially highly nonlinear [11]. In our study, we focus on BP NNs based on error back propagation learning algorithm proposed by Rumelhart et. al. in 1986, due to their strongly nonlinear mapping ability [43]. In general, BP NNs consist of an input layer, one or more hidden layers, and a output layer. The schematic diagram of the three-layers BP NNs containing one hidden layer is shows in Figure 4. The input layer in which no computation is carried out, has *L* nodes representing the length *L* of the input vector $\boldsymbol{X}$, is only used to input the input vector, then each node is connected to all *M* nodes of the hidden layer, each node in the hidden layer performs a nonlinear computation and is connected to each node of the output layer, the output vector $\boldsymbol{Z}$ containing *N* values is generated by a weighted sum over all of the output vector $\boldsymbol{Y}$ of the hidden layer [44].

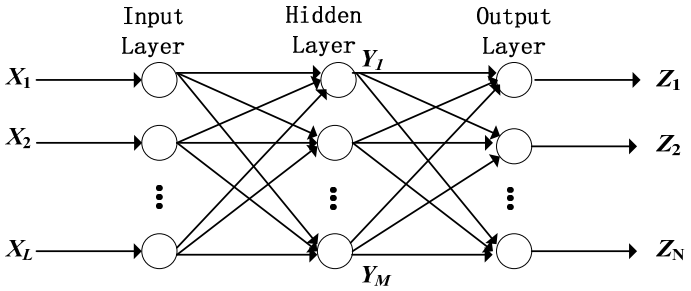

Figure 4. Diagram of BP Neural Networks.

The input vector $\boldsymbol{X}$ is carried out by a linear combine computation, followed by a nonlinear computation achieved through a nonlinear function (the so-called activation function), which can obtain an output of the hidden layer, given by

$$Y_j = S\left(\sum_{i=1}^{L} \omega_{ij} X_i + b_j\right), \tag{6}$$

where ω_{ij} is the connection weights between the *i*th input node and the *j*th hidden node, and b_j is the bias in the *j*th node of the hidden layer; *S*() is the activation function, sigmoidal function is selected, given by

$$S(a) = \frac{1}{1+e^{-a}}. \tag{7}$$

The output vector $\boldsymbol{Y}$ of the hidden layer input to a linear combiner to obtain the out vector $\boldsymbol{Z}$ of the output layer. At the training phase, The connection weights and bias in the BP NNs are adjusted iteratively to reduce the difference between the output vector of the pairs input/output vector and the calculated output vector estimated by the BP NNs using the input vector of the pairs input/output vector through the error back propagation algorithm which is described by Rumelhart et al. [43].

In our study, the differences of observations and simulations in the statistical analysis dataset in section 3.1 are taken as the output vector of the pairs input/output vector, and the corresponding atmospheric temperature and humidity profiles and skin temperatures are taken as the input vector of the pairs input/output vector (i. e. bias predictors), thus the length *L* of the input vector $\boldsymbol{X}$ is 74, and the length *N* of the output vector $\boldsymbol{Z}$ is 15 in the BP NNs. Based on many tests, the hidden layer with 30 hidden nodes was found to be best in our study. The connection weights and bias are determined through the training using 90% of the pairs input/output vector, the other 10% of pairs are used for validation to determine when to stop training.

Finally, based on the above analysis, we can get the correct brightness temperatures

$$O^*_j(\phi,\theta) = O_j(\phi,\theta) - d'_j(\phi,\theta) - Z_j(\phi,\theta). \tag{8}$$

where O^*_j are the correct brightness temperatures in channel *j*, O are the brightness temperatures without bias correction. In order to evaluate the effects of corrected brightness temperatures on the retrieval accuracy of atmospheric temperature and humidity profiles, we will build a physical retrieval system based on one-dimensional variational algorithm for MWHTS measurements.

4. Retrieval system for MWHTS

The retrieval system for MWHTS is based on the one-dimension variational algorithm, which is generally labeled under the general term of physical retrieval. one-dimension variational algorithm mainly includes two parts, one is the radiative transfer model for brightness temperature simulations, the other is the minimization of the following cost function:

$$J = \frac{1}{2}(x - x^b)^{\mathrm{T}} \boldsymbol{B}^{-1}(x - x^b) + \frac{1}{2}[H(x) - \boldsymbol{I}]^{\mathrm{T}} \boldsymbol{R}^{-1}[H(x) - \boldsymbol{I}], \tag{9}$$

which is the basics for the one-dimension variational algorithm, its purpose is weighting the relative contribution of background information and satellite observations. In equation (9), x^b is the background state variable and $\boldsymbol{B}$ is the background covariance matrix. $\boldsymbol{R}$ is the sum of the covariance error in the brightness temperature simulations and the sensor noise. T represents matrix transpose. H is the forward operator simulates the satellite observations at the atmospheric state variable x. $\boldsymbol{I}$ is the observations. Assuming the errors in the observations and the

Peer-reviewed version available at Atmosphere 2016, 7, 156; doi:10.3390/atmos7120156

background information are neither biased nor correlated, have Gaussian distributions, and assuming that there is a local linearity around x, the minimization of the cost function can be solved by:

$$\frac{\partial J}{\partial x} = 0. \tag{10}$$

This results in the solution x [45]:

$$x_{n+1} = x^b + \boldsymbol{B}\boldsymbol{H}^{\mathrm{T}}(x_n)[\boldsymbol{H}(x_n)\boldsymbol{B}\boldsymbol{H}^{\mathrm{T}}(x_n) + \boldsymbol{R}]^{-1}[\boldsymbol{I} - H(X) - (x^b - x_n)]. \tag{11}$$

where $\boldsymbol{H}$ is the tangent linear function of H at point x. n is the iteration index. As we can see from equation (11), the final solution x_{n+1} is affected by the priori information including the background covariance matrix B , the background state variable x^b and the first guess, the bias $\boldsymbol{I} - H(X)$ between observation and simulation, and the covariance matrix $\boldsymbol{R}$.

Duo to determine atmospheric state variable x from satellite observations is a underdetermined and ill-conditioned problem, it is important to use a source of a priori information to constrain the retrievals in iterative in equation (11) to within physically realistic solutions. In our study, we use the atmospheric temperature and humidity profiles from ERA-Interim reanalysis as described in section 3.1, but the time range is form 1 January to 30 December 2013, to generate background covariance matrix $\boldsymbol{B}$, The formula is given by [46]:

$$\sigma_{ij}^2 = \frac{1}{N}\sum_{i=1}^{N}\sum_{j=1}^{N}(x_i - \overline{x}_i)\times(x_j - \overline{x}_j), \tag{12}$$

where σ^2 is a element in the covariance matrix B, i and j represent the row and column, respectively. N is the number of the atmospheric temperature and humidity profiles used. We take the mean of the atmospheric temperature and humidity profiles for the calculations of background covariance matrix $\boldsymbol{B}$ in equation (12) as the background state variable x^b in our retrieval system. x_1 in equation (12) obtained from NWP model outputs is the first guess, the National Centers for Environmental Prediction (NCEP) Climate Forecast System (CFS) 6 h forecasts are used. The details of CFS are available in Saha et al. [47]. The same horizontal and temporal resolution of this data set as that of ERA Interim reanalysis and the collocated criteria with MWHTS measurements described in section 3.1 are selected.

For the bias $\boldsymbol{I} - H(X)$, The LRC and NNC methods proposed in section 3.2 are used to adjust the observed brightness temperatures. After removing biases in the observations, the standard deviation of observations to simulations and the sensitivities of MWHTS as measured in flight in Table 1 which is often considered as the instrument channel noise are used to compute the error covariance matrix $\boldsymbol{R}$ [48]. It is worth noting that different correction methods often correspond to different error covariance matrixes.

The convergence criterion adopted in our retrieval system is when

$$\frac{|J_{n+1} - J_n|}{J_n} < 0.01. \tag{13}$$

This mathematically means that the iteration is stopped if the relative difference of the cost function within two iterations is less than 0.01, and the maximum of 10 iterations is set, if the iterative times reach 10, the retrieval is set to the first guess. In addition, if the residuals between the measurements and those simulated by RTTOV from the first guess are greater than 20 K, then the measurements are abandoned. This is carried out for retrieval quality control.

Preprints (www.preprints.org) | NOT PEER-REVIEWED | Posted: 19 August 2016 doi:10.20944/preprints201608.0178.v1

Peer-reviewed version available at Atmosphere 2016, 7, 156; doi:10.3390/atmos7120156

5. Results

5.1. Bias correction results

LRC and NNC methods are applied to MWHTS observations coming from the testing dataset in section 3.1, with the bias predictors generated by the corresponding first guess used in the retrieval system built in section 4. Figure 5 shows the probability density distribution of brightness temperature biases for MWHTS channels 1-15 against the simulated brightness temperatures. For the MWHTS observations over ocean, the mean biases in channels 1-4, 6-8, 10 and 13-15 before bias correction are large, but have been significantly reduced and approaches zeros after both LRC and NNC methods. In addition, the probability density distribution of brightness temperature biases are more similar to a Gaussian distribution than that of before bias correction. This two bias correction both can get desired correction results. For the MWHTS observations over land, the biases of between brightness temperatures and simulated brightness temperatures in channels 2-7 and 11-15 can be effectively corrected by this two correction methods, and the effect of correction is about the same as that of over ocean. However, the biases correction in the other channels shows different behaviors using different correction methods. LRC cannot correct the biases and improve the probability density distribution of biases to make it obey a Gaussian distribution, thus it will be fail in the physical retrieval system. But the correction results by NNC are satisfied. The two correction methods shows different behaviors over ocean and land, this is may be mainly caused by the surface emissivity. The sea surface emissivity can be calculated accurately by the FASTEM-5 model, but due to greater variations in surface characteristics, the calculation of the land surface emissivity is complicated and the accuracy is always lower than that of sea surface emissivity, although the land surface emissivity atlas is used in our simulated calculations. In addition, the land surface has higher emissivity which cause the radiation from the surface and the atmosphere being close to the surface mixed, the channels 1 and 8-10 which are sensitive to the surface are difficult to distinguish whether the contribution is from land or atmosphere. This lead the relations of atmospheric parameters and the biases between observations and simulations much more complicated. Duo to the strong nonlinearity mapping ability of neural networks, NNC can represents this relations well, and get the better correction results than LRC.

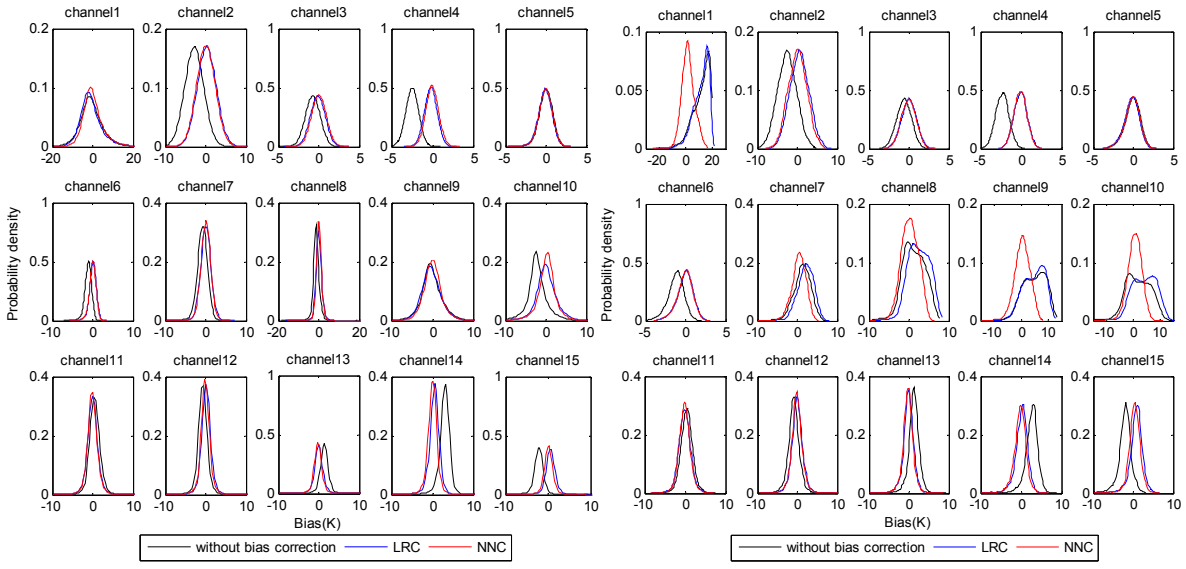

(a) (b)

Figure 5. Probability density distribution of brightness temperature biases for MWHTS channels 1-15 against the simulated brightness temperatures. (a) ocean, (b) land.

Preprints (www.preprints.org) | NOT PEER-REVIEWED | Posted: 19 August 2016 doi:10.20944/preprints201608.0178.v1

Peer-reviewed version available at Atmosphere 2016, 7, 156; doi:10.3390/atmos7120156

In order to quantitatively evaluate the performance of this two bias correction methods further, the RMSE is used as given below

$$RMSE = \sqrt{\frac{1}{N}\sum_{i=1}^{N}(x_i - y_i)^2} \,. \tag{14}$$

where x_i and y_i are the corrected and simulated brightness temperatures respectively, and N is the total number of comparisons. The RMSE of the biased before and after bias correction show in Figure 6. It can be seen that the RMSE of bias without bias correction is large over both ocean and land, especially in the channels 1 and 8-10 which are sensitive to the surface and the atmosphere closed to the surface. Over ocean, the RMSE of bias in all of channels corrected by the two correction approaches decrease obviously, the correction effect of NNC is better than that of LRC. but, over land, as expected, the correction effect of bias in channels 1 and 8-10 corrected by LRC is very poor, the RMSE of bias even larger than that of without bias correction. The RMSE of bias in temperature sounding channels 3-7 and water vapor sounding channels 11-15 are less than that of in channels 1 and 8-10, are within 1.5 K over both ocean and land, and NNC can get better correction effect. However, the RMSE of bias in channel 2 is still high, though it has reduced significantly using the correction methods. This may be related to the accuracy of atmospheric temperature profiles in the upper atmosphere.

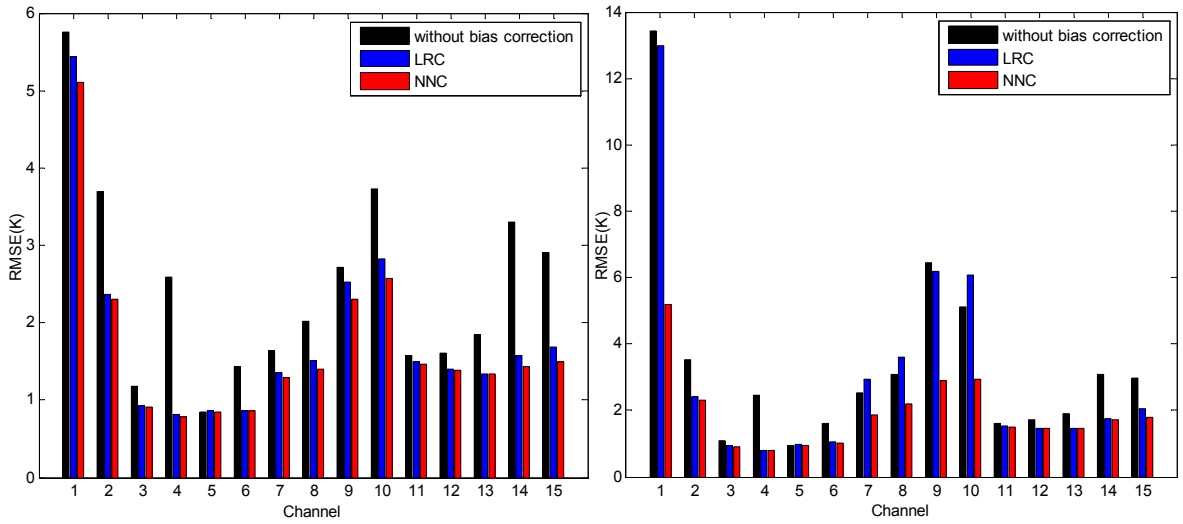

Figure 6. The RMSE of the biases before and after bias correction for MWHTS channels 1-15. (a) ocean, (b) land.

5.2. Results for MWHTS retrievals

An inversion of MWHTS measurements including the brightness temperatures with and without bias correction from the testing dataset in section 3.1, and the corresponding simulated brightness temperatures into atmospheric temperature and relative humidity profiles experiment was carried out to investigate the influences of LRC and NNC methods on the inversion accuracy. In our retrieval system, the iterative times are less than 5 in general. Duo to the retrieval quality control, more than 95% and 84% of solutions obtain convergence over ocean and land, respectively. In our study, RMSE is considered as the standard quantification to validate the retrievals with ECMWF ERA Interim reanalysis which is used as the truth. The RMSE is defined as equation (13), but the x_i and y_i are replaced by ECMWF reanalysis and MWHTS retrieved parameters respectively. Based on the MWHTS channels WFs analysis, we validate the retrievals at levels from 1000 to 20 hPa and 1000 to 250 hPa for temperature and relative humidity respectively. Figure 7 shows the RMSE of

inversion for ocean and land cases respectively. For the retrievals over ocean, the retrieved temperature RMSE using corrected measurements shows the substantial improvement over that of using measurements without bias correction from 200 to 20 hPa and 750 to 450 hPa in which the channels 2-4 and channels 6 are sensitivity to, the retrieval accuracy can be increased by 0.9 K. as can be seen from Figure 6(a), the correction results of this channels are good. However, the retrieved temperature accuracy using measurements corrected by NNC is better than that of using measurements by LRC at levels from 1000 to 800 hPa in which the correction results obtained by NNC outperformed that of the LRC, whose accuracy is similar to that of measurements without bias correction. Duo to the better performance of NNC method, the retrieved temperature accuracy is closer to the retrieved results using the simulated brightness temperatures. The retrieved humidity RMSE using measurements corrected by the two correction methods is significantly smaller than that of using measurements without bias correction, the retrieval accuracy can be increased by 6.8%. NNC method works better than LRC method, too. Compared with the retrieved results over ocean, we come to the same conclusion that the retrievals using corrected measurements has higher accuracy than that of the measurements without bias correction over land, the retrieval accuracy for temperature and humidity can increased by 0.8 K and 11% respectively, However, except for the temperature RMSE at levels from 1000 to 900 hPa where the channels 7-10 are sensitivity to, the retrieval accuracy of LRC is even lower than that of the measurements without bias correction, duo to the biases in channels 7-10 are still high as can be seen from Figure 6(b). It can be found from the retrieved RMSE both over ocean and land that the better bias correction results corresponds to the higher retrieval accuracy, the retrieval accuracy using measurements corrected by NNC is nearest to that of using simulated brightness temperatures, which is means that NNC method has better performance. One important thing to note about this retrieval results is that the temperature and humidity RMSE using simulated measurements is still large, this is caused by some other factors such as background covariance matrix, background state variable and first guess, investigating the effect of these factors on the retrieval accuracy and how to improve the retrievals are beyond of scope of our study in this paper, and will be study in a future publication.

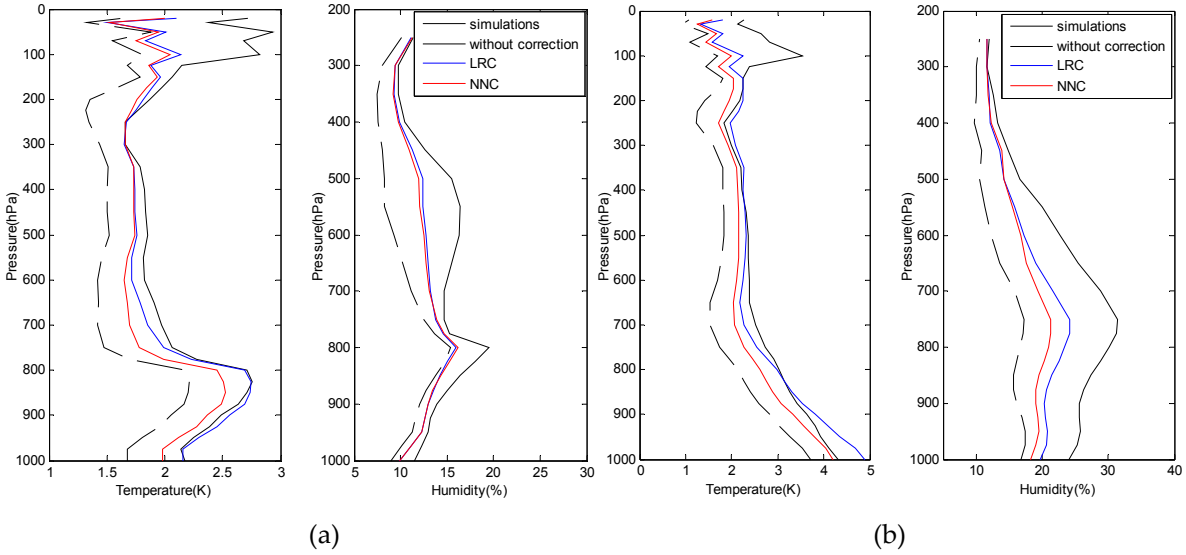

Figure 7. Temperature and relative humidity RMSE of retrieval over (a) ocean, (b) land.

5.3. Evaluation of algorithm robustness

From the analyses above, NNC method can provide excellent performance in the physical process. However, it's necessary to examine the algorithm performance when the atmospheric parameters used to generated the bias predictors fall outside the training dataset of NNs. we should note that the atmospheric parameters used to generated the bias predictors in the training phase of NNC come from ECMWF reanalysis dataset, but in the retrieval system built in our study, the first guess come

Preprints (www.preprints.org) | NOT PEER-REVIEWED | Posted: 19 August 2016 doi:10.20944/preprints201608.0178.v1

Peer-reviewed version available at Atmosphere 2016, 7, 156; doi:10.3390/atmos7120156

from the NCEP CFS forecast dataset as the bias predictors have achieved the desired correction results. There is reason to believe that better correction results can be obtain when the bias predictors generated by the atmospheric parameters come from the testing dataset in section 3.1. However, this cannot be realize in the retrieval system. Figure 8 shows the difference of RMSE of bias correction using the first guess as the bias predictors and that of using atmospheric parameters in the testing dataset in section 3.1. It can be seen that the differences of between the corrected results using atmospheric parameters come from different data sources are almost equal to zeros, except for the channels 1 and 7-10, in which of the observations are affected by the surface emissivity, however, the atmospheric parameters is used to calculated the surface emissivity may have a large amount of forecast error in the NCEP CFS 6 h forecasts, such as 10 m wind speed. Figure 9 shows the effects of the corrected results on the retrieval accuracy, the differences are too small to be statistically significant, thus the correction results biases caused by bias predictors using the different data sources in our retrieval system have little effect on the retrieval accuracy. This suggests that the performance of NNC method proposed in our study is fairly robust in the retrieval system.

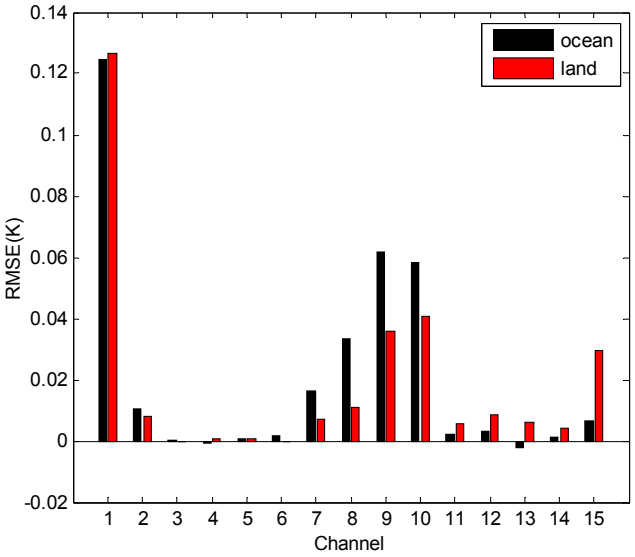

Figure 8. RMSE of bias correction using the first guess as the bias predictors minus RMSE of bias correction using the ECMWF reanalysis as the bias predictors.

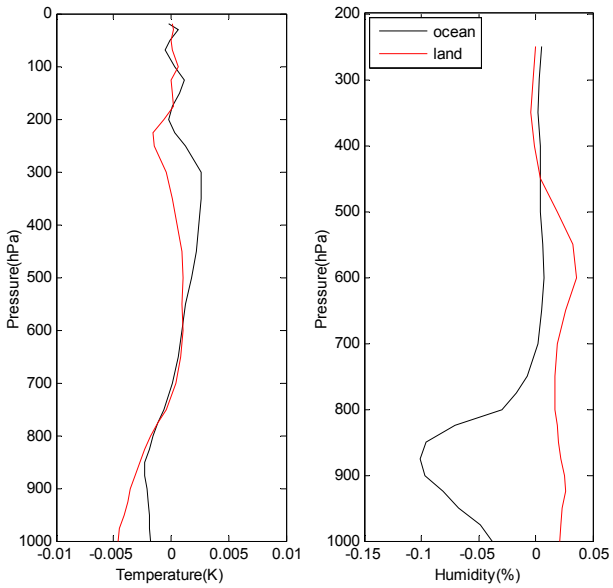

Figure 9. As Figure 8 but for retrieval accuracy.

5.4. Evaluation of algorithm stability

A well-constructed NNs can obtain the same solution which is not affected by the NNs initialization represented by the weights and biases used at the start of training. we can assess the stability of the algorithm through examining the solutions returned by NNC with different initialization states. we retrained the NNs of NNC with randomly initialized weights and biased four separate times, then applied this NNC method to the same MWHTS observations as that of section 5.1. Figure 10 shows the differences of RMSE of bias correction between four bias corrections and the NNC bias correction in section 5.1. It can be seen that the corrected results obtained by the four cases are similar to that of in section 5.1 both over ocean and land. The differences of RMSE of bias correction over land are greater than that of over ocean obviously because of affecting by surface emissivity accuracy, but the differences are too small to affect the retrieval accuracy in our inversion system which is the same as that of shown in Figure 9. This suggests that NNC method proposed in our study is insensitive to the initialization state.

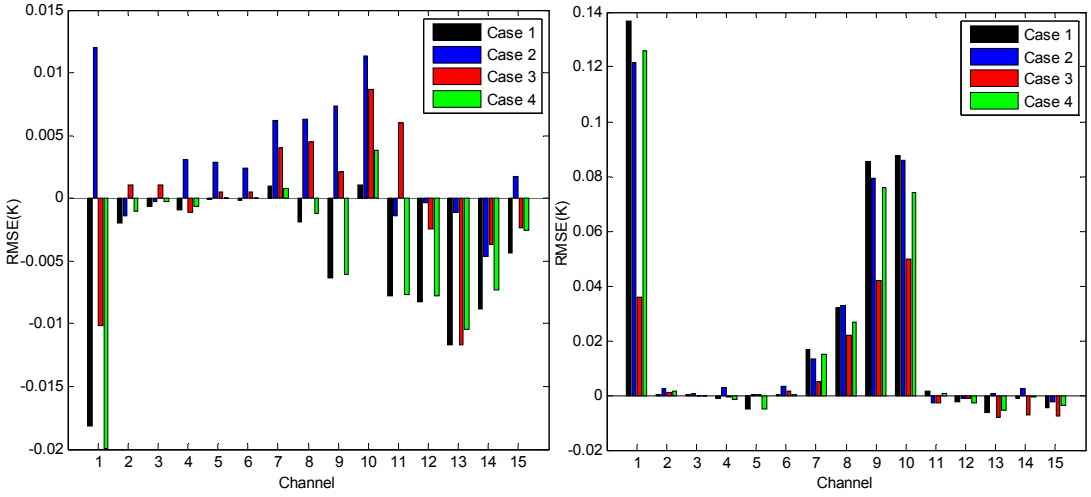

Figure 10. The differences of RMSE of bias correction between four bias corrections and the NNC bias correction in section 5.1.

6. Conclusions

In this works, two air mass correction methods have been proposed, LRC and NNC representing the linear and nonlinear nature between MWHTS measurements and air mass respectively, to correct the systemic biases between the MWHTS observations and simulations coming from radiative transfer model in the physical retrieval process. It has been shown that NNC method obtained the desired correction results outperformed LRC method, and incorporating such correction brightness temperatures in the one-dimensional variational system built in this study could obtain higher retrieval accuracies of atmospheric temperature and humidity profiles than that of LRC and without bias correction. This is also suggests that the better correction results can obtain the higher retrieval accuracy in the physical process. To fully assess the performances of NNC method, NNC is carried out with bias predictors from NCEP CFS forecasts which is used in the retrieval system and bias predictors from ECMWF reanalysis which is used in the training phase of NNs, respectively. the results of comparison suggests that NNC is fairly robust. The sensitivity of NNC to the initialization of the NNs at the start of training shows that NNC has high stability.

In conclusion, NNC method proposed in this paper is promising for the reason of representing the relationships of systemic bias and atmosphere state in the physical retrieval system or the statistical retrieval in which using simulations rather than the actual measurements irrespective of the collocated error between the satellite observations and atmospheric variables in time and space. Nevertheless, NNC is not suitable in NWP radiance assimilation system in which an adaptive bias correction scheme is preferred to distinguish satellite observation bias from NWP model bias and prevent the contamination of the observation bias estimates by systemic NWP model errors. In addition, one important thing to note about the retrieval system built in our

study is that the retrieved atmospheric temperature profile accuracy needs to be increased. How to improve the accuracy of the retrieval system will be studied in the future work.

Acknowledgments: The authors would like to thank ECMWF for providing reanalysis data, as well as NCEP for providing forecasts data. This work was supported by the key fostering project of National space science center, Chinese academy of sciences (No. Y62112f37s) and the National 863 Project of China (No. 2015AA8126027) .

Author Contributions: He Qiurui and Wang Zhenzhan designed the study; He Qiurui wrote the article; He Qiurui and He Jieying performed the experiments; Wang Zhenzhan presented some conclusions.

Conflicts of Interest: The authors declare no conflict of interest.

References

1. Ebell, K.; Orlandi, E.; Hünerbein, A.; Löhnert, U.; Crewell, S. Combining ground-based with satellite-based measurements in the atmospheric state retrieval: Assessment of the information content. *J. Geophys. Res.* **2013**, 118, 6940-6956.
2. Ahn, M. H.; Kim, M. J.; Chung, C. Y.; Suh, A. S. Operational implementation of the ATOVS processing procedure in KMA and its validation. *Adv. Atmos. Sci*. **2003**, 20, 398-414.
3. Miao, J.; Kunzi, K.; Heygster, G.; Lachlan-Cope, T. A.; Turner, J. Atmospheric water vapor over Antarctica derived from Special Sensor Microwave/Temperature 2 data. *J. Geophys. Res.* **2001,** 106, 10187-10203.
4. Duck, T. J. A microwave satellite water vapor column retrieval for polar winter conditions. *Atmos. Meas. Tech*. **2016**, *9*, 2241-2252.
5. Guo, Y.; Lu, N. M.; Qi, C. L.; Gu, S. Y.; Xu, J. M. Calibration and validation of microwave humidity and temperature sounder onboard FY-3C satellite. *Chinese. J. Geophys-Ch*. **2015**, 58, 20-31.
6. Polyakov, A.; Timofeyev, Y. M.; Virolainen, Y. Comparison of different techniques in atmospheric temperature-humidity sensing from space. *Int. J. Remote Sens*. **2014**, 35, 5899-5912.
7. Gohil, B. S.; Gairola, R. M.; Mathur, A. K.; Varma, A. K.; Mahesh, C.; Gangwar, R. K.; Pal, P. K. Algorithms for retrieving geophysical parameters from the MADRAS and SAPHIR sensors of the Megha-Tropiques satellite: Indian scenario. *Q. J. Roy. Meteor. Soc*. **2013**, 139, 954-963.
8. Rao, T. N.; Sunilkumar, K.; Jayaraman, A. Validation of humidity profiles obtained from SAPHIR, on-board Megha-Tropiques. *Curr Sci India.* **2013**, 104, 1635-1642.
9. Shi, L. Retrieval of atmospheric temperature profiles from AMSU-A measurements using a neural network approach. *J Atmos Ocean Tech*. **2001**, 18, 340-347.
10. Chen, H.; Jin, Y. Q. Data validation of Chinese microwave FY-3A for retrieval of atmospheric temperature and humidity profiles during Phoenix typhoon. *Int. J. Remote Sens*. **2011**, 32, 8541-8554.
11. Blackwell, W. J.; Chen, F. W. *Neural networks in atmospheric remote sensing*; Artech House, USA, **2009**.
12. Liu, D.; Lv, C.; Liu K.; Xie, Y.; Miao, J. Retrieval analysis of atmospheric water vapor for K-band ground-based hyperspectral microwave radiometer. *IEEE Trans. Geosci. Remote Sens. S*. **2014**, 11, 1835-1839.
13. Stähli, O.; Murk, A.; Kämpfer, N.; Mätzler, C.; Eriksson, P. Microwave radiometer to retrieve temperature profiles from the surface to the stratopause. *Atmos. Meas. Tech.* **2013**, 6, 2477-2494.
14. Bleisch, R.; Kämpfer, N.; Haefele, A. Retrieval of troposphere water vapor by using spectra of a 22 GHz radiometer. *Atmos. Meas. Tech.* **2011**, 4, 1891-1903.
15. Weng, F.; Zou, X.; Wang, X.; Yang, S.; Goldberg, M. D. Introduction to Suomi national polar-orbiting partnership advanced technology microwave sounder for numerical weather prediction and tropical cyclone applications. *J. Geophys. Res.* **2012**, 117.
16. Dee, D. P. Bias and data assimilation. *Q. J. Roy. Meteor. Soc*. **2005**, 131, 3323-3343.
17. Auligné, T.; McNally, A. P.; Dee, D. P. Adaptive bias correction for satellite data in a numerical weather prediction system. *Q. J. Roy. Meteor. Soc*. **2007**, 133, 631-642.
18. Susskind, J.; Rosenfield, J.; Reuter, D. An accurate radiative transfer model for use in the direct physical inversion of HIRS2 and MSU temperature sounding data. *J. Geophys. Res.* **1983**, 88, 8550-8568.
19. Smith, W. L.; Woolf H. M.; Hayden C. M.; Schreiner A. J. The physical retrieval TOVS Export Package, Technical Proceedings of the first TOVS study conference, University of Wisconsin, Austria. **1984**.
20. Weng, F.; Zhao, L.; Ferraro, R. R.; Poe, G.; Li, X.; Grody, N. C. Advanced microwave sounding unit cloud and precipitation algorithms. *Radio Sci*. **2003**, 38.

21. Li, J.; Wolf, W. W.; Menzel, W. P.; Zhang, W.; Huang, H. L.; Achtor, T. H. Global soundings of the atmosphere from ATOVS measurements: The algorithm and validation. *J. Appl. Meteorol*. **2000**, 39, 1248-1268.
22. Kelly, G. A.; Flobert, J. F. Radiance tuning, Technical Proceedings of the fourth TOVS study conference, University of Wisconsin, Austria. **1988**.
23. McMillin, L. M.; Crone, L. J.; Crosby, D. S. Adjusting satellite radiances by regression with an orthogonal transformation to a prior estimate. *J. Appl. Meteorol*. **1989**, 28, 969-975.
24. Uddstrom, M. Forward model errors. Technical Proceedings of the sixth TOVS study conference, University of Wisconsin, Austria. **1991**.
25. Harris, B. A.; Kelly, G. A satellite radiance-bias correction scheme for data assimilation. *Q. J. Roy. Meteor. Soc*. **2001**, 127, 1453-1468.
26. Dee, D. P. Variational bias correction of radiance data in the ECMWF system. Proceedings of workshop on assimilation of high spectral resolution sounders in NWP, Reading, UK. **2004**.
27. Dee, D. P. Bias and data assimilation. *Q. J. Roy. Meteor. Soc*. **2005**, 131, 3323-3343.
28. Auligné, T.; McNally, A. P.; Dee, D. P. Adaptive bias correction for satellite data in a numerical weather prediction system. *Q. J. Roy. Meteor. Soc*. **2007**, 133, 631-642.
29. Dee, D. P.; Uppala, S. Variational bias correction of satellite radiance data in the ERA-Interim reanalysis. *Q. J. Roy. Meteor. Soc*. **2009**, 135, 1830-1841.
30. Wu, C. Q.; Ma, G.; Qi, C. L.; Guo, Y.; You, R. Retrieval of atmospheric and surface parameters from VASS/FY-3C data under non-precipitation condition. SPIE Asia Pacific Remote Sensing . International Society for Optics and Photonics, Beijing, China. **2014**.
31. Liebe, H. J.; Hufford, G. A.; Cotton, M. G. Propagation modeling of moist air and suspended water/ice particles at frequencies below 1000 GHz. AGARD 52nd Specialists meeting of electromagnetic wave propagation panel, Palma De Mallorca, Spain. **1993**.
32. Karbou, F.; Aires, F.; Prigent, C.; Eymard, L. Potential of Advanced Microwave Sounding Unit-A (AMSU-A) and AMSU-B measurements for atmospheric temperature and humidity profiling over land. *J. Geophys. Res*. **2005**, 110.
33. Zou, X.; Wang, X.; Weng, F.; Li, G. Assessments of Chinese Fengyun Microwave Temperature Sounder (MWTS) measurements for weather and climate applications. *J. Atmos. Ocean. Tech.* **2011**, 28, 1206-1227.
34. Sivira, R.; Brogniez, H.; Mallet, C.; Oussar, Y. A layer-averaged relative humidity profile retrieval for microwave observations: design and results for the Megha-Tropiques payload. *Atmos. Meas. Tech.* **2015**, 8, 1055-1071.
35. Saunders, R.; Hocking, J.; Rundle, D.; Rayer, P.; Matricardi, M.; Geer, A.; Lupu, C.; Brunel, P.; Vidot, J. RTTOV-11 Science and validation report. *NWP-SAF report, Met. office, UK*, **2013**, 1-62.
36. Liu, Q.; English, S.; Weng, F. Fast microwave ocean emissivity model version 5 (FASTEM-5). *IEEE Trans. Geosci. Remote Sens*. **2012**, 50.
37. Aires, F.; Prigent, C.; Bernardo, F.; Jiménez, C.; Saunders, R.; Brunel, P. A Tool to Estimate Land-Surface Emissivities at Microwave frequencies (TELSEM) for use in numerical weather prediction. *Q. J. Roy. Meteor. Soc*. **2011**, 137, 690-699.
38. Berrisford, P.; Dee, D.; Poli, P.; Brugge, R.; Fielding, K.; Fuentes, M.; Kallberg, P.; Kobayashi, S.; Uppala, S.; Simmons, A. The ERA-Interim archive Version 2.0, ERA Report Series 1, ECMWF, Shinfield Park. *Reading, UK*, **2011**.
39. Buehler, S. A.; Kuvatov, M.; Sreerekha, T. R.; John, V. O.; Rydberg, B.; Eriksson, P.; Notholt, J. A cloud filtering method for microwave upper tropospheric humidity measurements. *Atmos. Chem. Phys.* **2007**, 7, 5531-5542.
40. Burns, B. A.; Wu, X.; Diak, G. R. Effects of precipitation and cloud ice on brightness temperatures in AMSU moisture channels. *IEEE Trans. Geosci. Remote Sens*. **1997**, 35, 1429-1437.
41. Greenwald, T. J.; Christopher, S.A. Effects of clod clouds on satellite measurements near 183 GHz. *J. Geophys. Res.* **2002**, 107, 4170.
42. Hong, G.; Heygster, G.; Miao, J.; Kunzi, K. Detection of tropical deep convective clouds from AMSU-B water vapor channels measurements. *J. Geophys. Res.* **2005**, 110, D05205.
43. Rumelhart, D. E.; Hinton, G. E.; Williams, R. J. *Learning internal representations by error propagation.* Technical Report, DTIC Doument, **1985**.

44. Yao, Z. G.; Chen, H. B.; Lin, L. F. Retrieving atmospheric temperature profiles from AMSU-A data with neural networks. *Adv. Atmos. Sci.* **2005**, 22, 606-616.
45. Liu, Q.; Weng, F. One-dimensional variational retrieval algorithm of temperature, water vapor, and cloud water profiles from advanced microwave sounding unit (AMSU). *IEEE Trans. Geosci. Remote Sens*. **2005**, 43, 1087-1095.
46. Boukabara, S. A.; Garrett, K.; Chen, W.; Iturbide-Sanchez, F.; Grassotti, C.; Kongoli, C.; Chen, R.; Liu, Q.; Yan, B.; Weng, F.; Ferraro, R.; Kleespies, T. J.; Meng, H. MiRS: An all-weather 1DVAR satellite data assimilation and retrieval system. *IEEE Trans. Geosci. Remote Sens*. **2011**, 49, 3249-3272.
47. Saha, S.; Moorthi, S.; Wu, X.; Wang, J.; Nadiga, S.; Tripp, P.; Behringer, D.; Hou, Y. T.; Chuang, H. Y.; Iredell, M.; Meng, J.; Yang, R. Q.; Mendez, M. P.; Van Den Dool, H.; Zhang, Q.; Wang, W. Q.; Chen, M. Y.; Becher, E. The NCEP climate forecast system version 2. *J. Climate*. **2014**, 27, 2185-2208.
48. English, S. J. Estimation of temperature and humidity profile information from microwave radiances over different surface types. *J. Appl. Meteorol*. **1999**, 38, 1526-1541.